J Nanostruct 15(4): 2553-2571, Autumn 2025

RESEARCH PAPER

Friendly Green Synthesis of Cerium Oxide Nanoparticles Using Citrus Aurantuim Extract and Applied in Removal of Eosin Yellow Dye

Forat Hamed Kadhem [1], Luma M. Ahmed [1,2] *, Salam A. Abed [3], Afraa Naji Tami [2], Wan Mohd Nuzul Hakimi Wan Salleh [4]

[1] *Department of Chemistry, College of Science, University of Kerbala, Karbala, Iraq*

[2] *Al-Zahraa Center for Medical and Pharmaceutical Research Sciences (ZCMRS), Al-Zahraa University for Women, Karbala, Iraq*

[3] *Department of Pharmacognosy, College of Pharmacy, University of Kerbala, Karbala, Iraq*

[4] *Department of Chemistry, Faculty of Science and Mathematics, Universiti Pendidikan Sultan Idris, Malaysia*

ARTICLE INFO

Article History:
Received 17 May 2025
Accepted 25 September 2025
Published 01 October 2025

Keywords:
Adsorption
Cerium oxide NPs
Citrus aurantuim
Green synthesis
Removal

ABSTRACT

Biosynthetic routes for producing nanoparticles have created a wide interest due to their environmental friendliness, simplicity, affordability, and clean technology. They do not contain hazardous chemicals or produce contaminants or byproducts. This work affords a green synthesis approach for cerium oxide nanoparticles CeO_2NP performed using hexane extract from *Citrus aurantuim* peels sourced from Karbala-Iraq. Gas Chromatography-Mass Spectrometry analysis of this hexane extract recognized key bioactive compounds inside the *Citrus aurantuim* peels extract, which included Limonene (35.72%), β-Pinene (25.43%), Myrcene (15.87%), and Linalool (12.34%) that elevated the stabilization of synthesis CeO_2NP. XRD of synthesis CeO_2NP revealed a cubic fluorite shape with a mean crystal size of 12nm. BET analysis indicated a specific floor area of 85.6 m^2/g and a mean pore diameter of 8.2 nm, ensuring a mesoporous structure. The perfect removal of 10 ppm of eosin yellow dye using 0.025 g of CeO_2 NPs turned into pH 6 at 90 min which agreed with zeta potential analysis, and the adsorption process followed pseudo-second-order kinetics. The ΔH^o of adsorption is 13.430 kJ/mol due to this reaction being physical adsorption. The reusability study showed the CeO_2NP could be successfully used up to the 3rd cycle before a loss of 50% from efficiency.

How to cite this article
Kadhem F., Ahmed L., Abed S., Tami A., Salleh W. Friendly Green Synthesis of Cerium Oxide Nanoparticles Using Citrus Aurantuim Extract and Applied in Removal of Eosin Yellow Dye. J Nanostruct, 2025; 15(4):2553-2571. DOI: 10.22052/JNS.2025.04.090

INTRODUCTION

Nanotechnology is a vital area of modern research that deals with the design, synthesis, and manipulation of particle structures ranging in size from 1 to 100 nm [1]. The prefix Nano is derived from the Greek word Nanos, which means "dwarf", and refers to one billionth10^{-9}m) in size [2]. Nanoparticles have numerous applications in fields such as health care, cosmetics, food and feed, environmental health, mechanics,

* *Corresponding Author Email: luma.ahmed@uokerbala.edu.iq*

optics, biomedical sciences, chemical industries and electronics, space industries, drug-gene delivery, energy science, electronics, catalysis, single-electron transistors, light emitters, nonlinear optical devices, and photoelectron chemical applications [3,4]. New advancements in nanotechnology are progressively driven by artificial intelligence (AI). Techniques like machine learning optimize synthesis processes, predict nanoparticle properties, and improve the material design. Hassan *et al.* highlighted how AI reduces resource use and fosters eco-friendly novelty, introductory new applications in environmental remediation, biomedicine, and energy storage [5]. There are numerous physical, chemical, biological, and hybrid methods for synthesizing various types of nanoparticles [6]. To synthesize NPs, the most common chemical approaches, such as chemical reduction using a variety of organic and inorganic reducing agents, electrochemical techniques, physicochemical reduction, and radiolysis, are widely used. The distinct properties of biologically synthesized NPs are preferred over physical-chemically produced nanomaterials [7,8]. Biologically synthesized nanoparticles hold great potential for advancing health care and environmental applications, offering eco-friendly and biocompatible solutions [9]. Green synthesis of NPs from metal ions is more eco-friendly, free of chemical contamination, less expensive, and safe for biological applications. Green chemistry allows us to obtain the necessary substance in the safest possible way. It provides the selection of raw materials and process schemes, which exclude harmful substances, and toxic and hazardous chemicals, and focuses on industrial processes that do not pollute the environment [10]**.** Currently, chemistry is witnessing a significant development with the emergence of a novel and comprehensive scientific trajectory known as "green" chemistry. The field of "green" chemistry encompasses various disciplines, including synthetic organic chemistry, analytical chemistry, physical chemistry, toxicology, microbiology, biotechnology, and engineering [11]**.** The goal of green chemistry is to develop technologies for more efficient chemical reactions. Green chemistry aims to prevent pollution in the very early stages of the planning and implementation of chemical processes and covers all types and aspects of chemical processes to minimize environmental risks [12]**.** The problems within the competence of green chemistry can be categorized into two main areas. The first relates to the processing and utilization of environmentally hazardous waste and by-products of the chemical industry [13,14] The second, more promising, involves the development of new industrial processes to eliminate or minimize the form In green chemistry, fundamentally new constructs such as ideal process, ideal product and ideal consumer are used, ideal process is a simple, eco-friendly, one-stage process, effective at the molecular level, with the use of renewable raw materials, which provides maximum yield, ideal product requires a minimum of energy and packaging, is safe, recyclable and fully degradable by microorganisms [15]**.** The green synthesis of CeO_2 NPs using *Citrus aurantuim* peel extract entails the discount of cerium ions by way of bioactive compounds present in the extract,

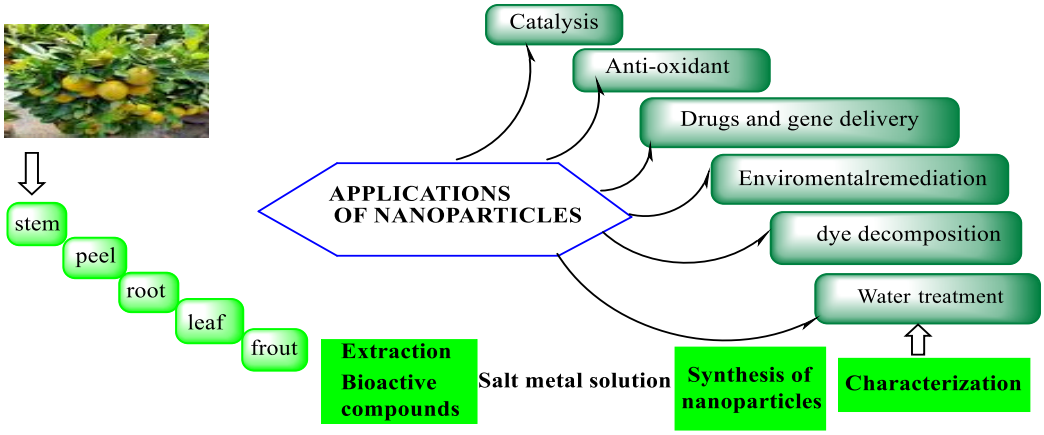

Fig. 1. Green synthesis of nanomaterial using Citrus aurantuim and application [13, 16].

which includes flavonoids and phenolic acids [16].The goal of this study is a green synthesis technique for cerium oxide (CeO_2) NPs using hexane extract from *Citrus aurantuim* peels. This method seeks to harness the natural antioxidant in the extraction beginning with the collection of fresh *Citrus aurantium* peels to provide CeO_2 NPs in a friendly environmental way. They take a look at will systematically look into the synthesis parameters to optimize the system, signify the ensuing nanoparticles in terms of size, crystallinity, and surface properties, and examine them in the removal of Eosin yellow dye. These studies have substantial implications for both nanotechnology and environmental sustainability as shown in Fig. 1.

MATERIALS AND METHODS

Materials, Reagents, and instrumentations

The source of *Citrus uranium* peels is Karbala, Iraq, which serves as the renewable uncooked fabric. Hexane purity of 99% facilitated the extraction of bioactive compounds supplied by (BDH, England). The cerium chloride ($CeCl_3.6H_2O$) purity of 99% was bought from (Merck, Germany). Ethanol purity of 99% and ammonia of 35% were purchased by (BDH). Eosin yellow dye ($C_{20}H_6Br_4Na_2O_5$) purity is 99% with acidic natural. The characterization of the nanoparticles was analyzed using a UV-visible spectrophotometer (UV-1900i, Shimadzu, Japan), Fourier Transform Infrared spectrophotometer (FT-IR) (IR Spirit, Shimadzu, Japan) using a KBr pellet with a scan rate of approximately 4 cm s^{-1} at 25 °C, field emission Scanning Electron Microscopy (Fe-SEM), Energy Dispersive X-ray spectroscopy (EDX) analysis (SU-8000, Hitachi, Japan) at accelerating voltages of 10 and 15 kV, and X-ray diffraction (XRD) (Rigaku Smart Lab spectrometer, Japan) with Cu-Kα radiation. A pH ION/EC/DO METER (MM-43X) was used to measure the pH of the solution.

Extraction of Citrus aurantuim peels

The extraction technique was started with the gathering of fresh *Citrus aurantuim* peels. Thorough washing the removal of impurities, and subsequent drying at room temperature for 48 hours were done to eliminate moisture. The dried peels (800g) were powdered using a mechanical grinder. Consequently, Soxhlet extraction was used to extract the bioactive compounds. Specifically, 370 g of the floor peel powder underwent extraction with 200 mL of hexane for 6 hours. Whatman No. 1 filter paper was used to filter the hexane extract to remove solid residues, and the extract was then concentrated, yielding an effective source of bioactive compounds. The steps of the bioactive compound extraction are displayed in Fig. 2.

Synthesis of CeO_2 Nanoparticles

The synthesis technique commenced with the

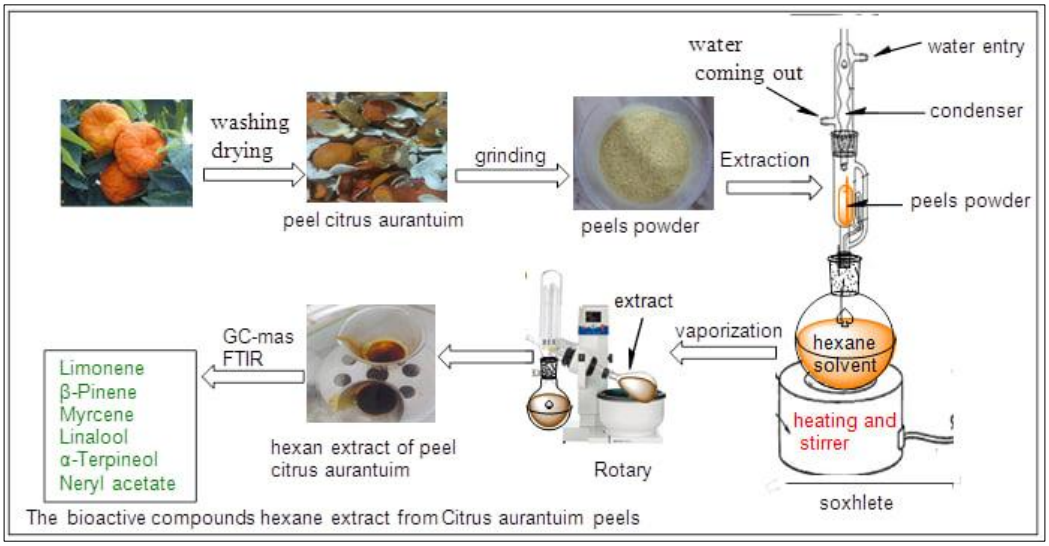

Fig. 2. The schematic diagram for the steps of the bioactive compounds extracted from *citrus aurantuim* peels in hexane.

dissolution of 4 g of cerium chloride ($CeCl_3.6H_2O$) in 100 mL of ethanol, making sure of complete dissolution via 10 min of stirring. Subsequently, 1g of the *Citrus aurantuim* peel extract was added, allowing the bioactive compounds to interact with the cerium ions as a template, capping agent, and stabilizer for 10 min beneath non-stop agitation. To facilitate oxide nanoparticle formation, the pH must be between 9 and 10, observed by adding drops of ammonia with stirring for 20 min. The heating process at 80°C for 3 hours with continuous stirring triggered was useful to grow the CeO_2 NP as a brown precipitate. The produced precipitate was washed with deionized water to cast off chloride ion residues. In this manner, to remove all chloride ions from the precipitate, must add drops of $AgNO_3$ solution to the filter. The produced CeO_2 was washed with ethanol to eliminate water and then dried at 60°C for 2h. Finally, the calcination of CeO_2 NPs yielded was performed at 600 °C for 3h to remove all organic compounds.

Removal of Eosin yellow dye using CeO_2 nanoparticles

Kinetic studies were done by taking different volumetric flasks and placing them in each of the 25 mL with a concentration range of (5,10,15 and 20) ppm of each of the adsorbed solutions of Eosin yellow dye. These solutions were contacted with (0.010, 0.015, 0,020, and 0.025) g of adsorbent surface (CeO_2 NPs), and then these flasks were placed in a water bath equipped with a vibrator at a different temperature within the range (283-298) K. The acid function for the removal process was adjusted within pH (3,4,5,6,7and 8). The flasks were then withdrawn at contact times between 15 min and 120 min, and the amount of adsorption was measured. The residue of Eosin yellow dye in solution after the adsorption process was measured at the maximum wavelength (λ_{max}) equal to 516 nm [17,18]. The adsorption capacity at various times qt in (mg/g) can be calculated using [19, 20]:

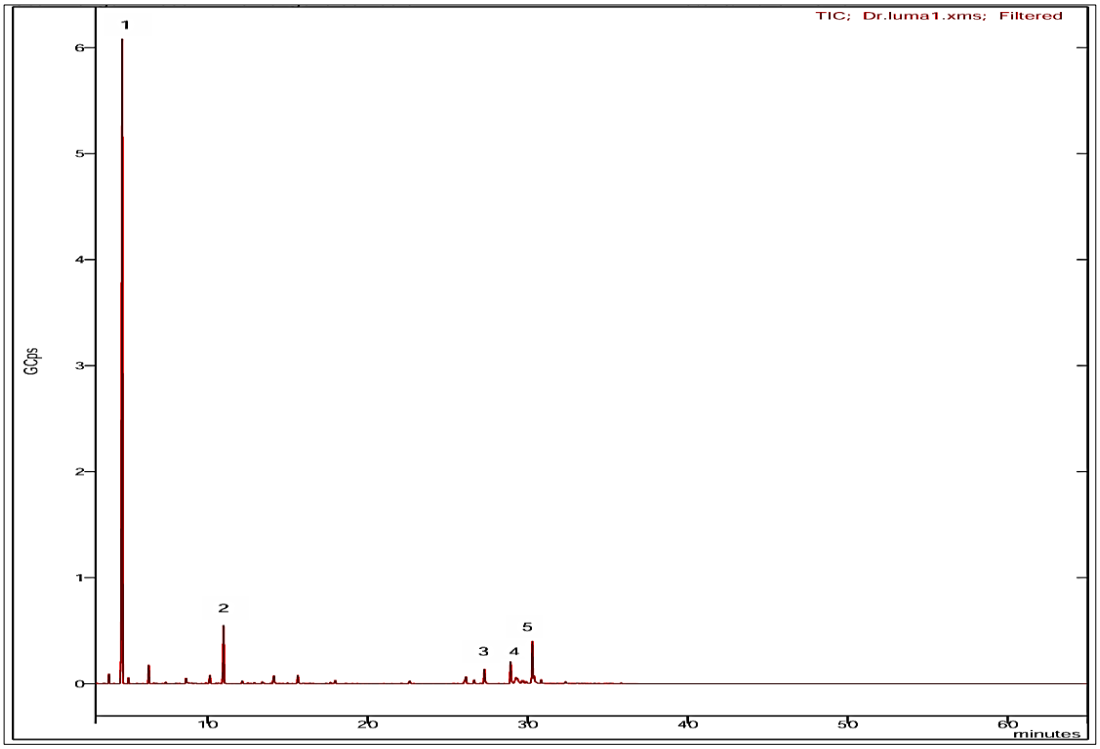

Fig. 3. Compounds Analysis of extract *Citrus aurantuim* peels by Retention Time Peak Area in (GC-MS) analysis.

$$q_t = \frac{(C_o - C_t)V}{m} \quad (1)$$

Where: C_o is the actual dye concentration in the solution, C_t is the concentration (mg/L) of dye at different times, V is the volume of the dye solution (L), and m is the mass of the adsorbent (CeO_2 NPs) used in (g).

The adsorption efficiency E % can be calculated by following the equation [21, 22]:

$$E\,\% = \frac{C_o - C_t}{C_o} x\,100 \quad (2)$$

The kinetic study of the adsorption of eosin yellow dye is evaluated by using the following equations depending on the adsorption capacity at equilibrium (q_e) as a maximum value in (mg/g) and adsorption capacity at various times qt in (mg/g).

a. *Pseudo –first-order kinetic: [23, 24]*

$$\ln (q_e - q_t) = \ln q_e - k_1\, t \quad (3)$$

Here: k_1: is the rate constant in (sec^{-1}) of pseudo-first order.

b. Pseudo-second order kinetic: [25,26].

$$\frac{1}{q_t} = \frac{1}{k_2 q_e^2} + \frac{1}{q_e} \quad (4)$$

Where: k_2:is the rate constant in ($L.M^{-1}.sec^{-1}$) of pseudo-second order.

RESULTS AND DISCUSSION

Characterization of extract Citrus aurantuim peels

Gas Chromatography-Mass Spectrometry (GC-MS) analysis was used to identify and quantify the bioactive compounds extracted from *Citrus aurantuim* peels. These compounds are essential oils as they facilitate the reduction and stabilization of CeO_2NPs during synthesis, as shown in Table 1 and Fig. 3.

The GC-MS analysis identified several key bioactive compounds in the *Citrus aurantuim* peel extract, GC/MS Analytical Condition, Injection: amount = 1µL Split ratio = 1:10 Heat of injection = 250 ℃, Column oven: initial temperature is 50 ℃ increase by 5 ℃ / min to 180 ℃ increase by 10 ℃ / min to 250 ℃ hold 1 min, Sample Preparation: 100 µL of the sample is diluted with 5 mL of N-Hexane (HPLC-Grade) before injection, and Gas flow ratio: 1 mL/min Pressure: 10 psi m/z Range:1 – 2000.

Limonene (35.72%) was the most abundant compound, followed by β-Pinene (25.43%), Myrcene (15.87%), and Linalool (12.34%). These compounds are known for their reducing and capping properties, which are essential in the green synthesis of nanoparticles. The presence of these compounds suggests their significant role in reducing cerium ions to CeO_2 NPs and stabilizing them against aggregation.

Characterization of CeO_2 nanoparticles

To comprehensively understand the properties and potential applications of the synthesized CeO_2 nanoparticles, a series of advanced characterization techniques were employed. These analyses included (FT-IR) spectroscopy, X-ray Diffraction (XRD), field emission Scanning Electron Microscopy (FE-SEM), Energy dispersive X-ray spectroscopy (EDX), Bruner–Emmett–Teller (BET) surface area analysis and Zeta potential analysis. Each technique provided valuable insights into the composition, structure, morphology, and surface characteristics of the nanoparticles, further elucidating their functional capabilities.

X-ray Diffraction (XRD)Analysis

XRD was performed to determine the crystalline structure of the synthesized CeO_2 NPs. The diffraction pattern provides information about

Table1. Gas Chromatography-Mass Spectrometry (GC-MS) analysis of extract *Citrus aurantuim* peels.

Retention Time (min)	Compound Name	Molecular Formula	Molecular Weight (g/mol)	Peak Area (%)
6.8	Limonene	$C_{10}H_{16}$	136.23	35.72
8.2	β-Pinene	$C_{10}H_{16}$	136.23	25.43
10.3	Myrcene	$C_{10}H_{16}$	136.23	15.87
12.6	Linalool	$C_{10}H_{18}O$	154.25	12.34
15.1	α-Terpineol	$C_{10}H_{18}O$	154.25	6.64
17.4	Neryl acetate	$C_{12}H_{20}O_2$	196.29	4.00

the phase and purity of the nanoparticles, as shown in Fig. 4. The XRD evaluation confirmed the crystalline nature of the nanoparticles, showing peaks corresponding to the cubic fluorite structure of CeO_2 NPs [27]. This crystalline shape is essential for the catalytic and biological activities of the nanoparticles because it enables the redox biking between Ce^{3+} and Ce^{4+} states [28, 29].

The characteristic peaks of the CeO_2 NPs correspond to the (111), (200), (220), (311), (222), and (400) planes. The strong peak at 28.6° for the (111) plane indicates a high degree of crystallinity and purity. The presence of these peaks confirms the formation of the cubic fluorite structure of CeO_2 NPs. The relative intensities of the peaks provide insights into the crystallographic orientation and crystal size [30]. The mean crystal size was calculated using the Scherer equation [30- 33].

$$D = \frac{k\lambda}{\beta\cos\theta} \quad (5)$$

Where *D* is the crystal size, *k* is the shape aspect (typically 0.9), *λ* is the X-ray wavelength (1.5406 Å for *Cu Kα*), *β* is the total width at half maximum (FWHM) of the height, and *ϑ* is the Bragg attitude, the calculated mean crystal size changed was found to be 12 nm.

FT-IR Analysis

The FTIR spectrum of the hexane extract was found to contain alcohols, phenols, aromatics, carboxylic acids, nitro compounds, and alkanes, as validated by the spectrum, as illustrated in Fig. 5A. A large peek at 3400-3600 cm^{-1} that attributed to O-H stretching vibrations, while another peak at 3051 cm^{-1} assignments to the N-H bending. The wide peak at 1408 cm^{-1} was observed, which was due to the bending of the O-H of carboxylic acid [34,35]. The peak demonstrated at 1627cm^{-1} is an attitude to the presence of C=O. The peak at 2850 cm^{-1} was assigned to C-H stretching, and the band at 1750 cm^{-1} corresponds to the bending of H–O–H which partly overlaps the O–C–O stretching band. The prominent absorption bands at 2927 and 1452 cm^{-1} are responsible for CH and CH_2 groups, respectively [36].

FTIR spectrum of CeO_2 NPs in Fig. 5B showed characteristic peaks. The new sharp peaks at 401 and 588 cm^{-1} indicative of Ce-O and O-Ce-O stretching vibrations, respectively [37,38].

FE-SEM Analysis

FE-SEM was used to observe the surface morphology and find the particle size of the synthesized CeO_2 NPs. This technique provides a high-resolution image that reveals detailed surface structure. FE-SEM images at different

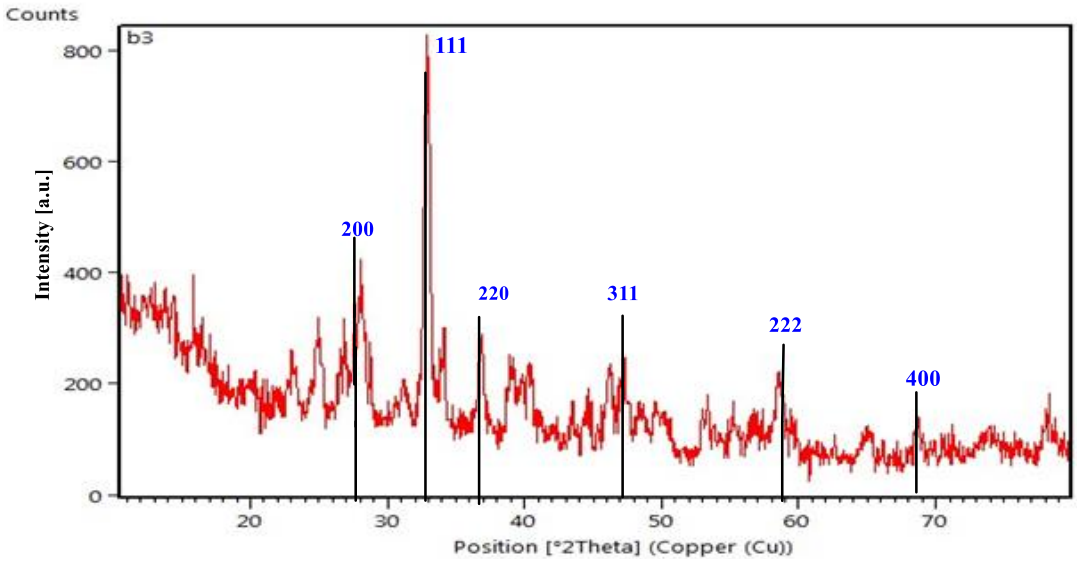

Fig. 4. XRD analysis of Green Synthesis of CeO_2 NP.

magnifications revealed that the CeO_2 NPs are predominantly spherical agglomerates like truffles, as shown in Fig. 6 A. At 10,000x magnification, the nanoparticles appeared well-dispersed with minimal aggregation.

At higher magnifications (20,000x) more detailed structures including clusters and surface textures were observed. The uniformity in shape and size suggests a controlled synthesis process, which is beneficial for applications requiring consistent nanoparticle characteristics. The particle size was determined to range between 29.3 nm and 45 nm. Based on Fig. 6B, the EDX spectrum demonstrated that the presence of cerium in the sample is found to be 62.6%, as well as the presence of oxygen observed at 25.5% and carbon at 12% resulting in the substrate material.

N_2 Adsorption - desorption isotherm (BET) Analysis

BET analysis was conducted to determine the specific surface area, total pore volume, and average pore diameter of CeO_2 nanoparticles. These parameters are critical for understanding the surface properties and potential catalytic activity of the nanoparticles. Based on Fig. 7A and B, the BET analysis revealed a specific surface area of 85.6 m^2/g, indicating a high surface area that is beneficial in catalytic applications. The total pore volume is found to be 0.35 cm^3/g and an average pore diameter is equal to 8.2 nm, these results suggest that the nanoparticles have a mesoporous structure [39]. This porosity enhances the accessibility of reactants to the active sites on the nanoparticle surface, making them suitable for various applications such as catalysis adsorption.

The adsorption isotherms classification is important in the theoretical modeling of adsorption phenomena and practical reasons. That considers the surface area measurements depending on the BET method [40]. The international standards use

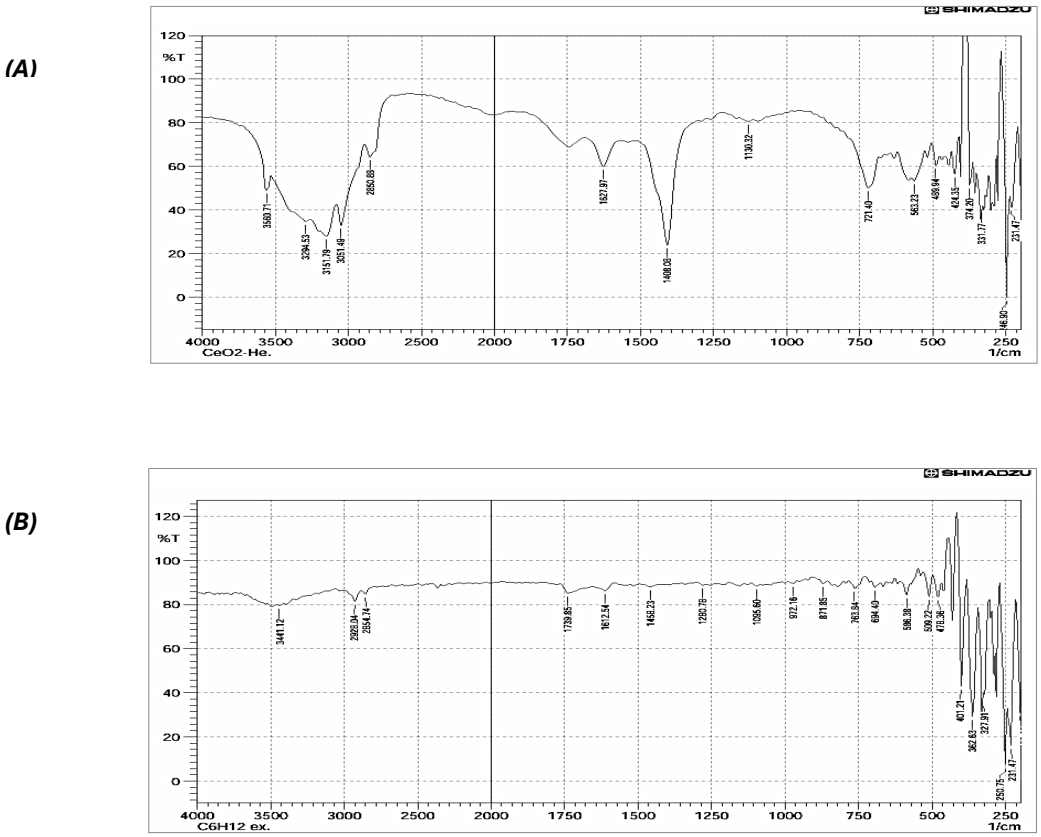

Fig. 5. FTIR spectra (A) *Citrus* peel extract with hexane and (B) CeO_2 NPs by using extract of peel *citrus aurantuim*.

this method in different applications depending on the first IUPAC manual [39,40], which divides the isotherms into five types. Fig. 7A is in agreement with Adsorption isotherms type IV, and the hysteresis loop was demonstrated in the relative pressure (P/P_0) range of 0.3~1.0, belonging to type H3 [39]. The expected pore is open with the shape may be as a cylinder [41].

Zeta Potential Analysis

Zeta potential analysis provides significant insights into the surface charge and colloidal stability of synthesized CeO_2 nanoparticles. The zeta potential is an important parameter affecting the diffusion and aggregation behavior of nanoparticles in solution [42]. The results of the zeta potential analysis are presented in Table 2.

At pH 3, CeO_2 NPs exhibited a zeta potential of +15.2 mV, indicating a moderate colloidal state. This positive charge indicates the presence of protonated surface groups, contributing to the electrostatic repulsion between the particles. At pH 6, the zeta potential increased sharply to +32.8 mV, indicating high stability[43]. This pH value is optimal for dispersion and prevention of aggregation of nanoparticles, which is useful for applications that require stable suspensions. At pH 8 the zeta potential is decreased and shifted to -21.4 mV, indicating good stability due to negative surface charge. The negative charge is apparently due to the de-protonation of the surface hydroxyl groups, resulting in explosive forces that prevent aggregation.

Adsorption of Eosin Yellow Dye

The synthesized CeO_2 NPs using *Citrus aurantuim* peel extract were evaluated to remove the Eosin yellow dye. The adsorption efficiency and kinetic adsorption constant (kd) were calculated at various time intervals, pH levels, temperatures, and initial dye concentrations. The mechanism of dye removal is shown in Fig. 8.

Effect of Removal Time

The data in Fig. 9 elucidates the temporal evolution of Eosin yellow dye adsorption by the synthesized CeO_2 nanoparticles. A substantial increase in the efficiency of dye removal and the adsorption constant values over time signifies the effective adsorption of the dye, this behavior is due to an increase in the kinetic energy for dye particles that enhances the diffusion and adsorption on active sites of the CeO_2NP surface until saturated[44]. The adsorption efficiency increased significantly from 26.18% at the initial 15 min to 70.66% after 120 min. Simultaneously,

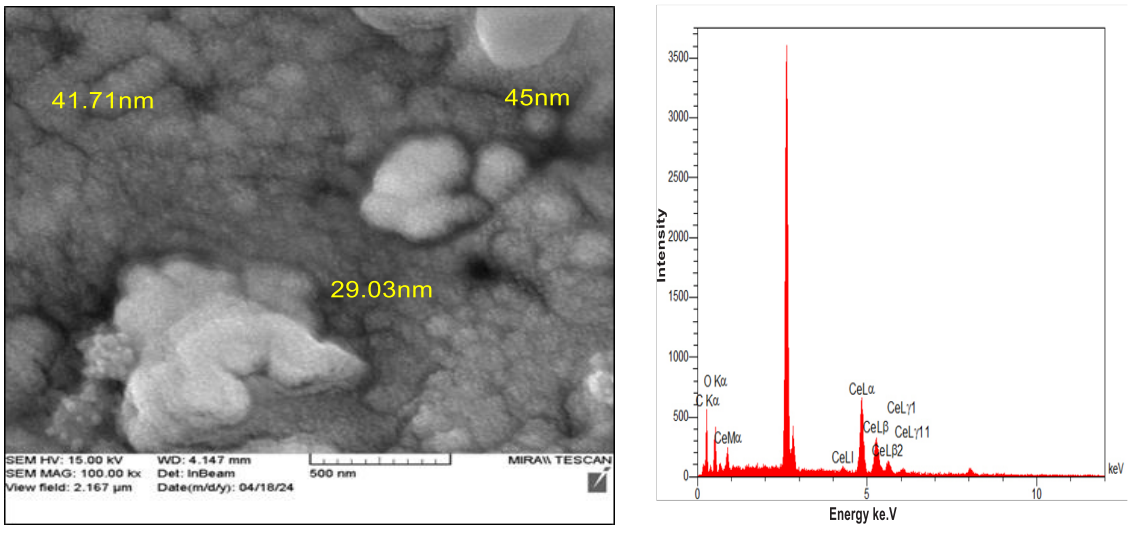

(A) (B)

Fig. 6. A) FE-SEM micrographs of Green Synthesis CeO_2 NP and B) EDX spectrum of Green Synthesis CeO_2 NP.

the adsorption constant (kd) increased, peaking at 2.4270 min^{-1} at 90 min and staying similar with continuous time.

The kinetic results as shown in Fig. 10 and Table 3. The values of the correlation coefficients for the pseudo-second-order model are relatively high, and the amount of adsorbed material calculated by this model is close to the value determined by experiments. The value of the correlation coefficient for the pseudo-first-order model of the adsorption system is not convincing. Therefore, the pseudo-second-order model is more accepter for describing the adsorption kinetic, so the rate-limited step depends on the Eosin yellow dye molecule and the CeO_2 nanoparticles surface.

Effect of Initial Dye Concentration on the Removal Process

The influence of varying initial dye concentrations on the adsorption process is encapsulated in Fig. 11 a discernible inverse relationship emerges between the initial dye concentration and the adsorption efficiency after increasing the dye concentration by more than 10 ppm. Specifically, the maximum efficiency was found at a concentration of 10 mg/L yielded an impressive 70.82%, while efficiencies decreased by using high concentrations, which reached 20 mg/L, resulting in a substantial to 26.58%. This observation can be attributed to the limited availability of active sites on the nanoparticle

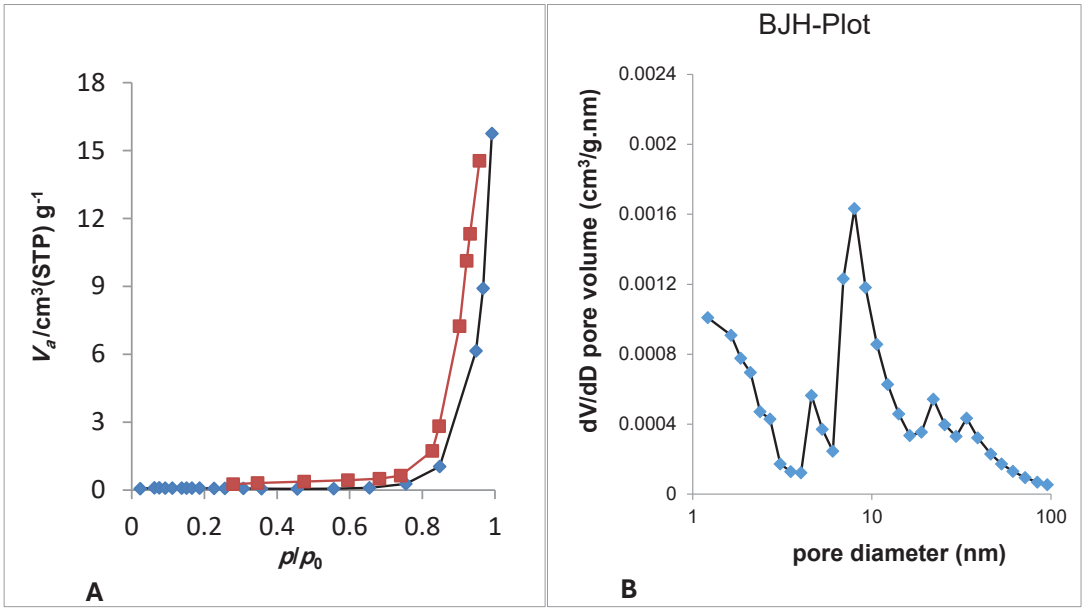

Fig. 7. (A) N_2 adsorption-desorption isotherms of Green Synthesis CeO_2 nanoparticles. (B) the corresponding Barrett-Joyner-Halenda pore size distribution curve of Green Synthesis CeO_2 nanoparticles.

Table 2. Zeta Potential Analysis of Green Synthesis CeO_2 nanoparticles.

Sample	pH	Zeta Potential (mV)	Stability
	3	+15.2	Moderate
CeO_2-NP	6	+32.8	High
	8	-21.4	Good

surface at higher dye concentrations, thereby hindering the adsorption and subsequent adsorption process [45,46]. Consequently, optimizing the initial dye concentration is crucial to maximize the potential of CeO_2 nanoparticles.

Effect of CeO_2 NP Dose

Fig. 12 encapsulates the effect of various dosages of CeO_2 NPs at the adsorption method. A clear positive correlation emerges between the nanoparticle dose and the adsorption performance, with the best efficiency of 70.82% achieved at a dose of 0.025 g. This trend may be attributed to the improved availability of energetic sites at the nanoparticle surface, which helps greater efficient adsorption and next adsorption of the dye molecules. However, it is crucial to strike a balance between the nanoparticle dosage and the associated costs, as an immoderate dose might not yield commensurate enhancements

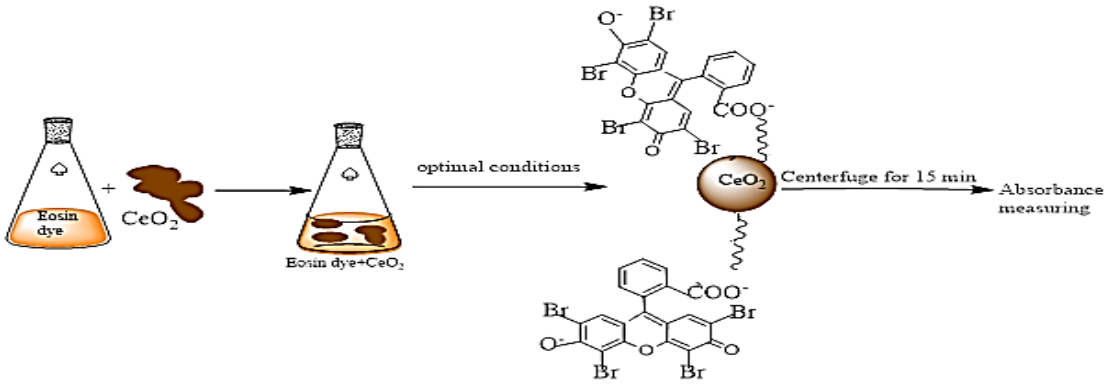

Fig. 8. Mechanism of eosin yellow dye removal using CeO_2 NP surface.

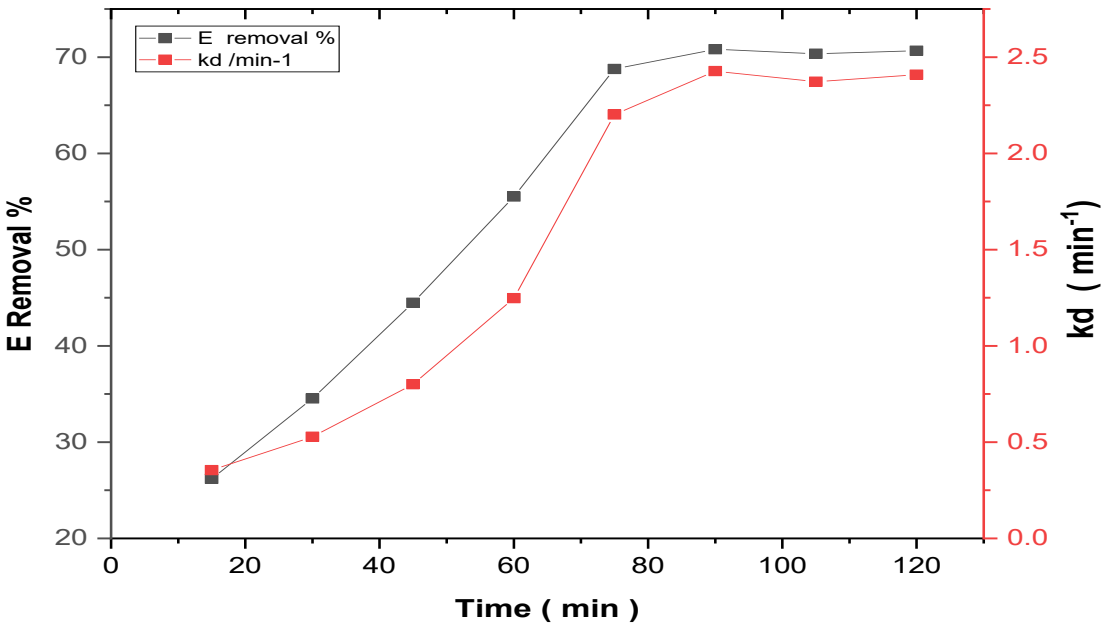

Fig. 9. Relationship of E% and kd contact vs time (min) for adsorption of Eosin yellow dye on green synthesis CeO_2 nanoparticles surface at initial pH equal to 8.

in efficiency. The results show that increasing the dosage of CeO_2 NPs led to higher adsorption efficiencies, with the best result observed at a dose of 0.025 g. The increase in the removal of dyes with adsorbent dose is due to the introduction of more binding sites for adsorption [47, 48].

Thermodynamic Parameters

Thermodynamic characteristics are essential for determining the kind of adsorption process that occurs on any solid surface. The thermodynamics parameters such as activation energy, Gibb's free energy change, entropy, and isotherm heat of

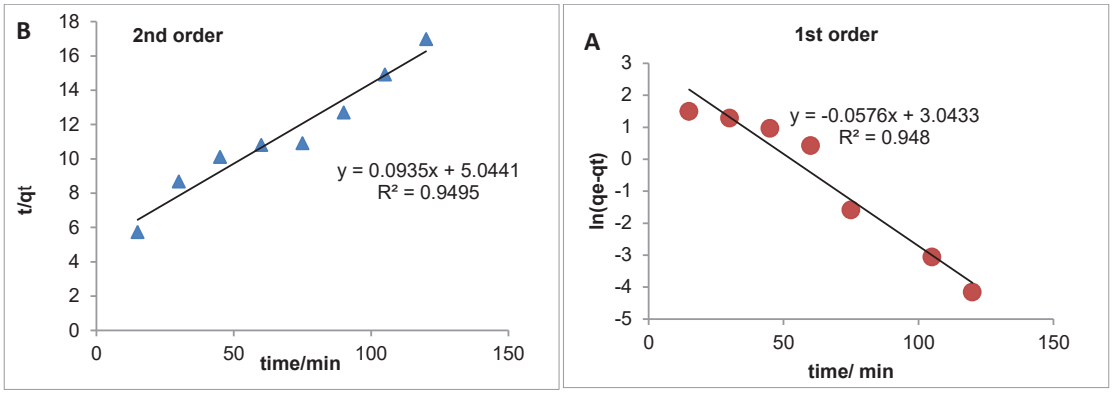

Fig. 10. A: Pseudo- first order B: Pseudo- second order kinetic study of Eosin yellow dye adsorption on CeO_2NPs surface at 298 K at initial pH equal to 8.

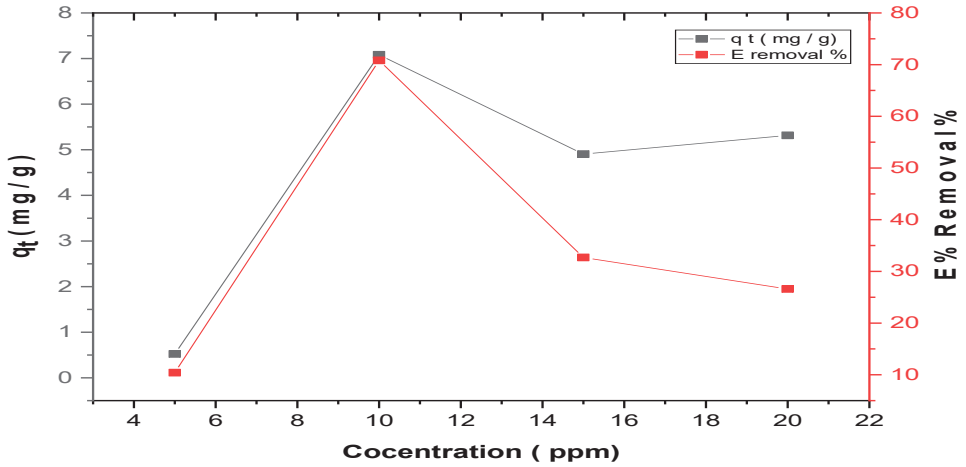

Fig. 11. Effect of Initial concentration of Eosin Yellow Dye on adsorption process by green synthesis of CeO_2 NPs at initial pH equal to 8.

Table 3. The kinetic results of pseudo-first-order and pseudo-second order reaction parameters of Eosin yellow dye on the CeO_2 NPs surface.

Samples	Pseudo-first order			Pseudo-second order		
	$k_1(min^{-1})$	$q_{e(mg/g)}$	R^2	$k_{2\ (g/mg.min)}$	$q_{e(mg/g)}$	R^2
CeO_2 NP	0.0576	20.97434	0.948	0.00173	10.6951	0.9495

adsorption are vitally required. These parameters are critical design variables in estimating the performance and predicting the mechanism of an adsorption separation process First, using equation 7, the sorption distribution coefficient (kd) [49,50] was determined.

$$k_{d=}\frac{C_{ads}}{C_e} \quad (6)$$

where C_{ads} is the amount of adsorbate (dye) on the solid surface equilibrium (mg/L) and Ce is the amount of leftover dye (mg/L) in an equilibrium solution.

The Van't Hoff formula was used to estimate the changes in the standard entropy ΔS° and the standard enthalpy ΔH° [51, 52], as shown in Fig. 13A.

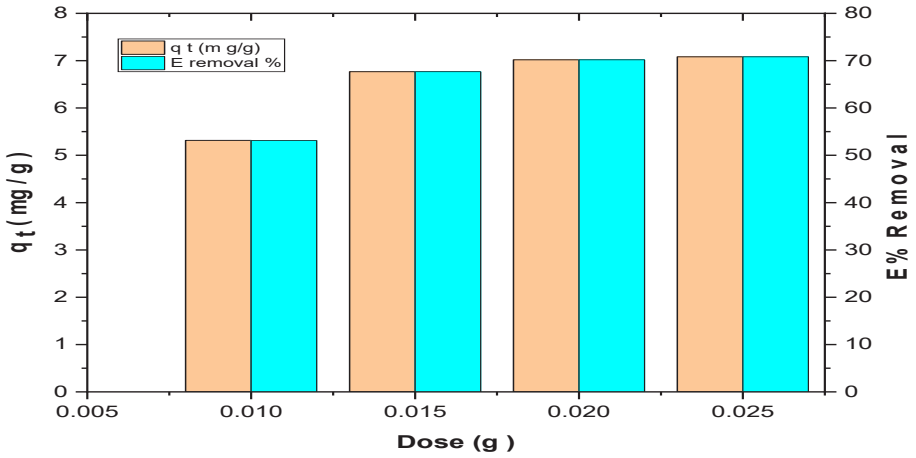

Fig. 12. Effect of Initial concentration of Eosin Yellow Dye on adsorption process by green synthesis of CeO_2 NPs at initial pH equal to 8.

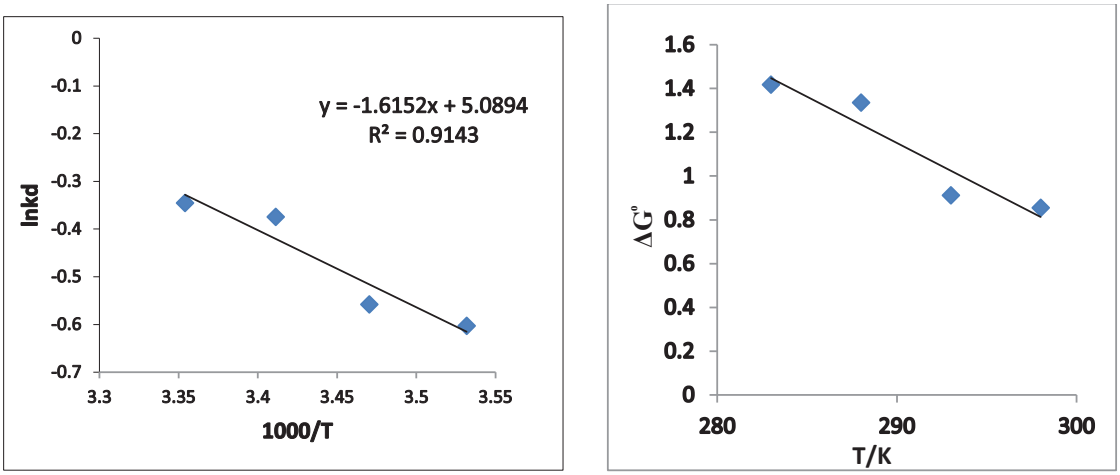

Fig. 13. (A)Relation between ln kd and (1000/T) and (B) Relation of ΔG° versus temperature for an endothermic process of Eosin yellow dye adsorption on green synthesis CeO_2 NPs surface at initial pH equal to 8.

$$\ln k_d = \frac{-\Delta H^o}{RT} + \frac{\Delta S^o}{R} \quad (7)$$

Here, R stands for the universal gas constant (J/mol. K) and T is the absolute temperature in Kelvin.

Using the Nernst equation (equation 9), the standard Gibbs free energy (ΔG°) was determined [53,54], and the relation between ΔG° and temperature is plotted in Fig. 13B.

$$\Delta G^o = -RT\ln k_d \quad (8)$$

However, equation) 10(was used to get the activation energy (Ea) [55].

$$E_a = \Delta H^o + RT \quad (9)$$

Based on Figs. 13A and B, Table 3 elucidates the thermodynamic parameters predominated on the adsorption manner. The Gibbs free energy (ΔG°) values are positive indicating the adsorption of Eosin yellow dye by green synthesized CeO_2 NP is a non-spontaneous reaction. The positive ΔH° of this reaction was found to be 13.430 kJ/mol, this value suggests that the adsorption type of the adsorption is physical (ΔH° less than 20-40 kJ/mol) and the system is endothermic [56]. Furthermore, the small value of ΔS^o (0.0423 kJ/mol. K) ensures the decline in the randomness of the solid-solution interface in the course of the adsorption system [57].

Effect of pH of Eosin dye on the Adsorption Process

This parameter shall describe via many phenomena that can be happened, which caused the change in surface charge properties of the nanoparticles and the solubility or ionization state of dye. Fig. 14 encapsulates the pivotal role of pH in modulating the adsorption of Eosin yellow dye.

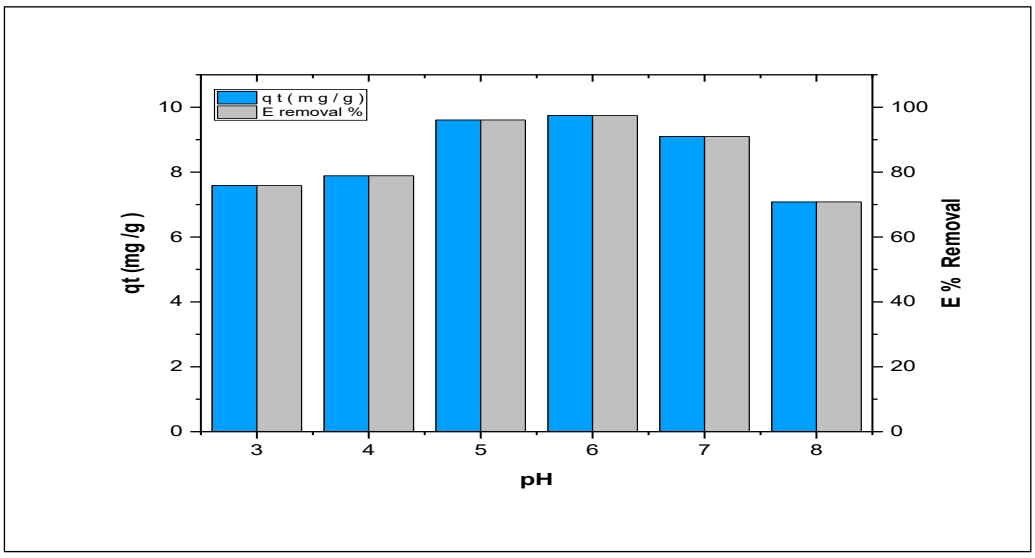

Fig. 14. Effect of initial pH of Eosin yellow dye on adsorption process using green synthesis CeO_2 NP.

Table 4. The Thermodynamic Parameters for Eosin yellow dye adsorption on green synthesis of CeO_2 NP surface at (283-298) K.

Temperature ^oC	Temperature (K)	1/T K^{-1}	kd min^{-1}	ln kd	ΔH° kJ/mol	ΔS° kJ/mol.K	ΔG° kJ/mol
10	283	0.00353	0.5473	-0.6027	13.430	0.0423	1.4181
15	288	0.00347	0.5726	-0.5576			1.3352
20	293	0.00341	0.6877	-0.3744			0.9121
25	298	0.00336	0.7082	-0.3450			0.8548

The efficiency increases from pH 3 to pH 6 and gives a maximum adsorption efficiency 97.48%. The results indicate the maximum adsorption efficiency at pH 6 was accepted with the result of zeta potential at maximum value at pH 6. The protonation of surface enhances the anionic dye adsorption owing to the electrostatic attraction [58]**.** Conversely, the adsorption efficiency diminished from pH 7 to 8 that attitude to excess the hydroxyl ions in surface that increases the repulsive force with this negative dye [59].

Adsorption Isotherms

In this study, we used Freundlich, Langmuir, and Temkin's isotherm equations to match the experimental data for eliminating eosin dye at different concentrations. The adsorption isotherm describes the relationship between the amount of removed dye and the remaining concentration at equilibrium. This work used non-linear Langmuir and Freundlich models to analyze adsorption isotherm data and characterize the process. The monolayer adsorption of the adsorbate on homogeneous sites within the adsorbent is characterized as:

Isotherm Langmuir

Definition of Langmuir isotherm (Equation10) states the adsorption process takes place across homogeneous sites of the adsorbent [60].

$$Q_e = \frac{abC_e}{1 + bC_e} \quad (10)$$

Where; Q*e* = defined as the quantity of eosin yellow adsorption at the time of equilibrium(mg/g). (a, b) are the constants of Langmuir.

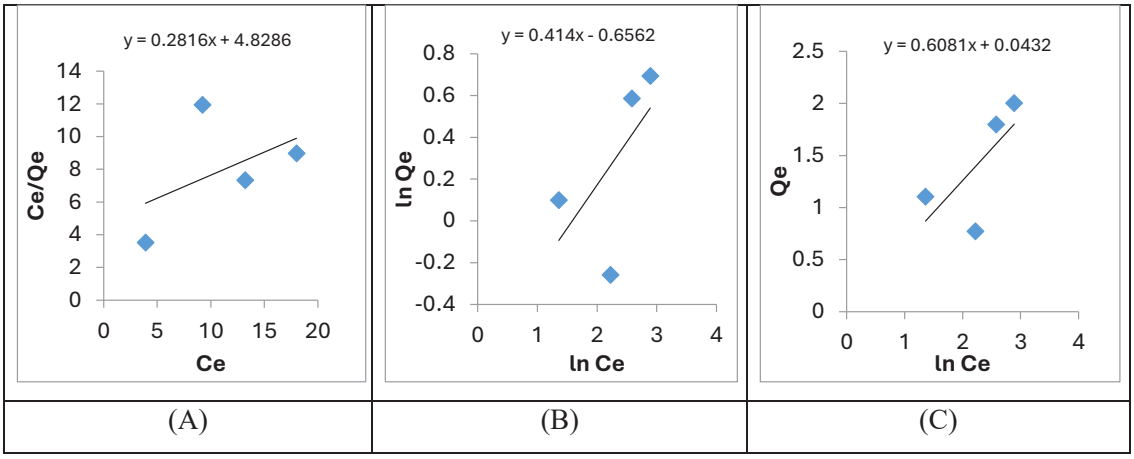

Fig. 15. A) Langmuir isotherms for eosin yellow dye using the surface of the CeO_2 NPs at 25°C, B) Freundlich isotherm eosin yellow dye using surface the CeO_2 NPs at 25°C and C) Temkin isotherm eosin yellow dye using the surface of the CeO_2 NPs at 25 °C.

Table 5. Adsorption isotherm values each of Langmuir, Freundlich, and Temkin at 25 °C.

Models	Langmuir isotherm	Models	Freundlich isotherm	Models	Tekmin isotherm
a (L/mg)	0.058336	KF	0.807833	β	0.5447
b (mg/g)	3.550128	n	3.19081	A_T	1.613490751
R_L	0.461528	R^2	0.4103	R^2	0.483
R^2	0.2307				

$$R_L = \frac{1}{1 + bC_e} \quad (11)$$

Where: RL = meaning refer to adsorption kinds is Irreversible (R_L=0), Likely (0< R_L< 1) linear (R_L=1) [56]. The (a) and (b) values are calculated from the slopes (1/a) and intercepts (1/ab) of linear plots of Ce /Qe versus Ce are shown in Fig. 15A.

Isotherm Freundlich

Multi-layered adsorption over heterogeneous active sites is indicated by the Freundlich isotherm pattern of adsorption. Freundlich isothermal. [57].

$$\mathrm{Log}Q_e = \mathrm{Log}K_F + \frac{1}{n}\mathrm{Log}C_e \quad (12)$$

Where: k_F, n =Freundlich's constants. Fig. 15B shows the applicability of the Freundlich equation well when plotting Log Qe against the values of Log Ce

Temkin Isotherm

The following is how it is frequently used [57]:

$$Q_e = \beta \ln A_T + \beta \ln C_e \quad (13)$$

Where: A_T is the equilibrium binding constant. β = associated with the heat of adsorption. where the eosin yellow dye adsorption Temkin isotherm curves are shown in Fig. 15C.

The (a, b, RL) for Langmuir constants, (n, KF) for the Freundlich pattern and the Temkin pattern constants (β, AT) with linear correlation coefficients are shown in Table 5.

From the results the (R^2) values in Table 5 for Langmuir, Freundlich and Temkin it turns out that the best results are in the Freundlich and Temkin values [60,61]. The Freundlich constant n is found to equal 3.198 that agreement with the actual this reaction is a multilayer (physical adsorption) and this process is favorable for the studied dye because the n value ranges between 1 and 10 [62]. The RL value is obtained less than 1, hence this reaction is Likely [60]. The R^2 is low which indicates the adsorption of dye on the surface of CeO_2 NP is heterogeneous.

Effect of Addition the Oxidation Agents on Eosin yellow dye removal process

Fig. 16 encapsulates have an impact on supplementary oxidizing dealers, specifically hydrogen peroxide (H_2O_2) and ferrous ions (Fe^{2+}), at the adsorption of eosin yellow dye. The records show that the addition of these oxidizing agents enhanced the adsorption performance, with the Fenton response (related to both H_2O_2 and Fe^{2+}) yielding an outstanding efficiency of 96.37%. This synergistic effect may be ascribed to the era of especially reactive hydroxyl radicals (•OH)

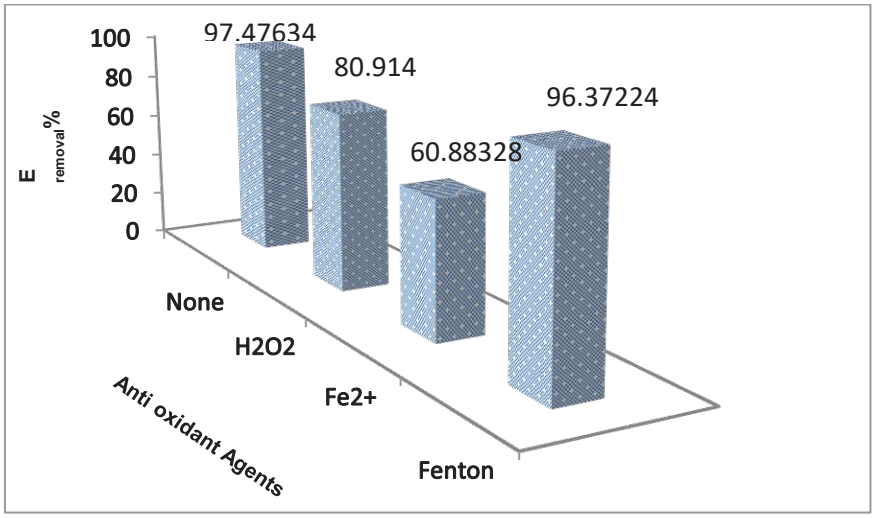

Fig. 16. Effect of oxidizing agents on adsorption efficiency of eosin yellow dye on green synthesis CeO_2 NPs surface at initial pH equal to 6.

through the Fenton technique, which augments the oxidative adsorption of the dye molecules. Consequently, the judicious incorporation of such oxidizing agents presents a viable strategy to further optimize the adsorption performance of the CeO_2 nanoparticles. The results indicate that the addition of hydrogen peroxide alone and ferrous ions alone depress the adsorption efficiency. This behavior due to the Fe^{2+} may be compared to the dye on occupies active sites in the cerium oxide nanoparticles via the adsorption process. Moreover, the H_2O_2 shall oxide the semiconductor surface to give a positive charge with hydroxyl ion and hydroxyl radical, and the last species will adsorption on the surface and decrease the negative dye adsorption (eosin yellow dye) this result is in agreement with result that reported in reference [63,64]. Whereas, using the Fenton reaction, which involves both H_2O_2 and Fe^{2+} resulted in an adsorption efficiency of 96.37%, very close to the efficiency observed without any additional oxidizing agents to generate equivalent positive and negative charges at the same time. As in the following equations [63-65].

$$Fe^{2+} + H_2O_2 \rightarrow Fe^{3+} + HO^- \quad (14)$$

$$HO^- + H_2O_2 \rightarrow HO_2 + H_2O \quad (15)$$

$$Fe^{3+} + HO_2^{\cdot} \rightarrow Fe^{2+} + H^+ + O_2 \quad (16)$$

$$Fe^{2+} + HO_2^{\cdot} \rightarrow Fe^{3+} + HO_2 \quad (17)$$

$$Fe^{2+} + HO^{\cdot} \rightarrow Fe^{3+} + HO^- \quad (18)$$

$$HO_2 + HO^{\cdot} \rightarrow H_2O + O_2 \quad (19)$$

Reusability of CeO_2 nanoparticles

The statistics provided in Fig. 17 shed mild on the reusability of the synthesized CeO_2 NPs for packages. While the nanoparticles exhibited an impressive 97.48 % removal efficiency performance in the preliminary cycle, a gradual decline in performance was found with subsequent reuse cycles. This phenomenon can be ascribed to the capacity deactivation by saturated or blocking the active sites of surface by dye molecules, or fouling of the nanoparticle surface, which may restrict the adsorption and adsorption strategies [66]. Nevertheless, the nanoparticle's proven ability to perform well during the first three rounds pastime more than one cycle underscores their potential for sustainable and fee-effective applications. The results indicate a decline in adsorption efficiency with a continuous reuse cycle when used five times. it maintained its warranty until the third time because the dye molecules are gradually accumulating and preventing interaction with

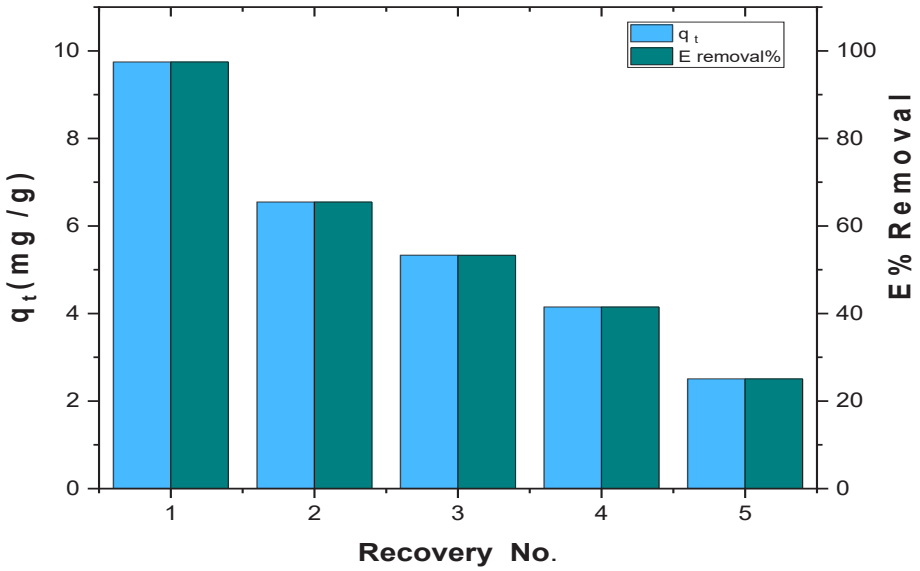

Fig. 17. Reusability of CeO_2 NPs surface for Eosin yellow dye adsorption at initial pH equal to 8.

the surface [67,68]. However, the nanoparticles still exhibited significant adsorption activity after multiple cycles. The results observed good reusability, which is the acceptable loss in the sorption ability after five circulations.

CONCLUSION

Green synthesis of CeO_2 NPs using *Citrus aurantuim* peel extract was successfully prepared and it provided a sustainable and environmentally friendly method. The synthesized CeO_2 NP was characterized by X-ray diffraction (XRD), field emission scanning electron microscopy (FE-SEM), Energy dispersive X-ray spectroscopy (EDX), Bruner–Emmett–Teller (BET) surface area analysis and Zeta potential analysis. Based on the XRD data, the CeO_2 NP structure was estimated as a cubic fluorite with a crystal size of 12 nm. The nanoparticles demonstrated good adsorption and antioxidant properties, making them suitable for a wide range of applications and emphasizing the need for further research to fully exploit their advantages. Based on kinetic studies and isothermal fitting, the second-order model was investigated as an appropriate model to express the adsorption behavior of dye on synthesized CeO_2 NP. The thermodynamic study indicated that the adsorption mechanism between synthesized CeO_2 NP and Eosin yellow dye was non- spontaneous and endothermic process. The Adsorption activity was studied by way of the preliminary dye concentration, pH, and temperature. Higher adsorption efficiencies were located at 10ppm dye concentrations, with a finest pH of 6, and multiplied interest at 25˚C temperature. Additionally, the green synthesis technique by leveraging agricultural –products, this observation aims to contribute to sustainable improvement and pollutant reduction, at the same time as exploring the practical packages of green–synthesized CeO_2 NPs in various fields such as environmental remediation. Research into the future Environmentally friendly and non-toxic preparation of Cerium oxide nanoparticles, including green synthesis. Characterize produced surfaces with TEM, TGA, and XPS to determine surface properties and bending energy. Investigating the impact of several parameters on adsorption, including ionic strength, and shaking speed. Examined the biological activity of produced materials.

ACKNOWLEDGMENTS

The authors would like to thank all supported people at the University of Karbala and Al-Zahraa Center for Medical and Pharmaceutical Research Sciences (ZCMRS), Al-Zahraa University for Women.

CONFLICT OF INTEREST

The authors declare that there is no conflict of interests regarding the publication of this manuscript.

REFERENCES

1. Mohammed N, Nawar S, Etawy M, Nassar G, Hassabo A. Nanotechnology and its Applications in Industry and Product Design. Journal of Textiles, Coloration and Polymer Science. 2024;0(0):0-0.
2. Rey T. Contributions to the Mathematical and Numerical Analysis of Multiscale Kinetic Equations (Doctoral dissertation, Université de Lille).2023.
3. Patel J, Kumar GS, Roy H, Maddiboyina B, Leporatti S, Bohara RA. From nature to nanomedicine: bioengineered metallic nanoparticles bridge the gap for medical applications. Discover Nano. 2024;19(1).
4. Carbó-Ramírez P, Zuria I, Schaefer HM, Santiago-Alarcon D. Avian haemosporidians at three environmentally contrasting urban greenspaces. Journal of Urban Ecology. 2017;3(1).
5. Hassan,S.A., Almaliki, M. N., Hussein, Z. A., Albehadili, H. M., Banoon, S. R., Al-Abboodi, A., Al-Saady, M. (2023). Development of Nanotechnology by Artificial Intelligence: A Comprehensive Review. Journal of Nanostructures.;13(4), 915-932.
6. Charbgoo F, Ahmad M, Darroudi M. Cerium oxide nanoparticles: green synthesis and biological applications. International Journal of Nanomedicine. 2017;Volume 12:1401-1413.
7. Emmanuel, O., Ahmad, M., Ezeji, T. C., Qureshi, N., & Abidin, S. Z. U. (2024). Bioenergy production from waste seed oil biomass of Cupressus sempervirens: A strategy for reducing environmental pollution. Sustainable Chemistry One World, 2, 100008.
8. Naidi SN, Harunsani MH, Tan AL, Khan MM. Green-synthesized CeO_2 nanoparticles for photocatalytic, antimicrobial, antioxidant and cytotoxicity activities. Journal of Materials Chemistry B. 2021;9(28):5599-5620.
9. Ali, Z. H., Al-Saady, M. A., Aldujaili, N. H., Banoon, S. R., Abboodi, A..(2022). Evaluation of the Antibacterial Inhibitory Activity of Chitosan Nanoparticles Biosynthesized by Streptococcus thermophilus. Journal of Nanostructures. 12(3), 675-685.
10. Polat DÇ, Karadağ AE, Köprülü REP, Karantas ID, Mutlu G, Çağlar EŞ, et al. Phytochemical Compounds Loaded to Nanocarriers as Potential Therapeutic Substances for Alzheimer's Disease-Could They be Effective? Curr Pharm Des. 2022;28(30):2437-2460.
11. Lancaster, M., 2025. Green chemistry: an introductory text. Royal society of chemistry.
12. Cormier SA, Lomnicki S, Backes W, Dellinger B. Origin and Health Impacts of Emissions of Toxic By-Products and Fine

Particles from Combustion and Thermal Treatment of Hazardous Wastes and Materials. Environ Health Perspect. 2006;114(6):810-817.
13. Aseyd Nezhad S, Es-haghi A, Tabrizi MH. Green synthesis of cerium oxide nanoparticle using Origanum majorana L. leaf extract, its characterization and biological activities. Appl Organomet Chem. 2019;34(2).
14. Bhati M. Biogenic synthesis of metallic nanoparticles: Principles and applications. Materials Today: Proceedings. 2023;81:882-887.
15. Pansambal S, Oza R, Borgave S, Chauhan A, Bardapurkar P, Vyas S, et al. Bioengineered cerium oxide (CeO_2) nanoparticles and their diverse applications: a review. Applied Nanoscience. 2022;13(9):6067-6092.
16. Hamed SM, El Tablawy NH, Mohamed MYA, Alammari BS, AbdElgawad H. Accumulation and nano-ecotoxicological impact of cerium oxide nanoparticles on cyanobacteria: Understanding photosynthesis, detoxification, and antioxidant responses. Journal of Environmental Chemical Engineering. 2024;12(2):112134.
17. Jawad TM, Ahmed LM. Direct Ultrasonic Synthesis of WO_3/TiO_2 Nanocomposites And Applying Them in the Photodecolorization of Eosin Yellow Dye. Periódico Tchê Química. 2020;17(34):621-633.
18. Ahmed LM. Photo-Decolourization Kinetics of Acid Red 87 Dye in ZnO Suspension Under Different Types of UV-A Light. Asian J Chem. 2018;30(9):2134-2140.
19. Saati M, Hamidi S, Jarolmasjed N, Rezvani Z, Davari S. Preparation of Novel CeO_2/Nio/Nial2o4 Nanocomposite for Fast and Efficient Removal of Direct Red 23: Mechanism, Kinetic, Thermodynamic and Equilibrium Studies. SSRN Electronic Journal. 2022.
20. Jawad TM, R. Al-Lami M, Hasan A, Al-Hilifi J, Mohammad R, Ahmed L. Synergistic Effect of dark and photoreactions on the removal and photo-decolorization of azo carmosine dye (E122) as food dye using Rutile- TiO2 suspension. Egyptian Journal of Chemistry. 2021;0(0):0-0.
21. Ahmed H, Elsayed A. Enhancement of wool fabric dyeing via treatment with AgNPs. Egyptian Journal of Chemistry. 2020;0(0):0-0.
22. Mohammad, H. M., Saeed, S. I., & Ahmed, L. M. (2022). Broccolilike iron oxide nanoparticles synthesis in presence of surfactants and using them in the removal of water-colored contamination. Journal of Nanostructures, 12(4), 1034-1048.
23. Athab ZH, Halbus AF, Mohammed SB, Atiyah AJ, Ismael HI, Saddam NS, et al. Comparison activity of pure and chromium-doped nickel oxide nanoparticles for the selective removal of dyes from water. Sci Rep. 2024;14(1).
24. Serban GV, Iancu VI, Dinu C, Tenea A, Vasilache N, Cristea I, et al. Removal Efficiency and Adsorption Kinetics of Methyl Orange from Wastewater by Commercial Activated Carbon. Sustainability. 2023;15(17):12939.
25. Ali, S., Ali, M., & Ahmed, L. (2021). Hybrid Phosphotungstic Acid-Dopamine (PTA-DA) Like-flower Nanostructure Synthesis as a Furosemide Drug Delivery System and Kinetic Study of Drug Releasing. Egyptian Journal of Chemistry, 64(10), 5547-5553.
26. Al-Khafaji E. Synthesis and Characterization of Ni/Al-LDH nano hybrid with (Ascorbic acid) and Kinetic Controlled Release Study of (Ascorbic acid) From Ni/Al-LDH. Journal of Physics: Conference Series. 2020;1660(1):012026.
27. Taresh, B. H., Fakhri, F.H., & Ahmed, L. M. (2022). Synthesis and Characterization of CuO/CeO2 Nanocomposites and Investigation Their Photocatalytic Activity. Journal of Nanostructures, 12(3), 563-570.
28. Singh KRB, Nayak V, Sarkar T, Singh RP. Cerium oxide nanoparticles: properties, biosynthesis and biomedical application. RSC Advances. 2020;10(45):27194-27214.
29. Fifere N, Airinei A, Dobromir M, Sacarescu L, Dunca SI. Revealing the Effect of Synthesis Conditions on the Structural, Optical, and Antibacterial Properties of Cerium Oxide Nanoparticles. Nanomaterials. 2021;11(10):2596.
30. Khariri, A.A., Rahaju, A.A., & Mustika, A.A. (2021).The Effect of Mixed Liquor Administration on The Johnsen's Score and The Number of Sertoli Cells and Leydig Cells on The Wistar Strain White Rats (Rattus norvegicus). Indian Journal of Forensic Medicine & Toxicology, 15(1).
31. Jaafar, M. T., Ahmed, L. M., and Haiwal, R. T.(2023). Solvent-free hydrothermal synthesis of network-like graphene quantum dots (GQD) nano particle and ultrasonic TiO_2-GQD nanocomposite. Journal of Nanostructures. 13(3), 626-638.
32. Al-khafaji EN, Mathkoor MM, Al-Anbari HH. Preparation and Characterization of Silver Nanoparticles Using Rosemary and Olive Leaf Aqueous Extracts. IOP Conference Series: Earth and Environmental Science. 2023;1158(10):102002.
33. Hammod, I.A., Ridha, N.J., Tahir, K.J., Alosfur, F.K.M. and Yasir, A.S., (2024). Effects of Concentration on the Sensing Properties of Rgo/CuO Nanoparticles as Ammonia Gas Sensor. Nanotechnology Perceptions. 514-529.
34. Arunachalam T, Karpagasundaram M, Rajarathinam N. Ultrasound assisted green synthesis of cerium oxide nanoparticles using Prosopis juliflora leaf extract and their structural, optical and antibacterial properties. Materials Science-Poland. 2017;35(4):791-798.
35. Prabaharan DMDM, Sadaiyandi K, Mahendran M, Sagadevan S. Structural, Optical, Morphological and Dielectric Properties of Cerium Oxide Nanoparticles. Materials Research. 2016;19(2):478-482.
36. Parvathy S, Manjula G, Balachandar R, Subbaiya R. Green synthesis and characterization of cerium oxide nanoparticles from Artabotrys hexapetalus leaf extract and its antibacterial and anticancer properties. Mater Lett. 2022;314:131811.
37. Tumkur PP, Gunasekaran NK, Lamani BR, Nazario Bayon N, Prabhakaran K, Hall JC, et al. Cerium Oxide Nanoparticles: Synthesis and Characterization for Biosafe Applications. Nanomanufacturing. 2021;1(3):176-189.
38. Putri, G.E., Rilda, Y., Syukri, S., Labanni, A. and Arief, S., (2021). Highly antimicrobial activity of cerium oxide nanoparticles synthesized using Moringa oleifera leaf extract by a rapid green precipitation method. Journal of Materials Research and Technology, 15, pp.2355-2364.
39. Donohue MD, Aranovich GL. Classification of Gibbs adsorption isotherms. Advances in Colloid and Interface Science. 1998;76-77:137-152.
40. Ambroz F, Macdonald TJ, Martis V, Parkin IP. Evaluation of the BET Theory for the Characterization of Meso and Microporous MOFs. Small Methods. 2018;2(11).
41. de Boer, J. H., The Dynamical Character of Adsorption (Oxford University Press, Oxford, 1953.
42. Thomas SP, Mansoor HHA, Kullappan M, Sethumathavan V, Natesan B. Effect of Zeta Potential on Chitosan Doped Cerium Oxide in the Decolorization of Cationic Dye under Visible Light Irradiation. Fibers and Polymers. 2019;20(7):1418-1423.

43. Clogston JD, Patri AK. Zeta Potential Measurement. Methods in Molecular Biology: Humana Press; 2010. p. 63-70.
44. Abdullah RH, Majeed AS, Nehaba SS, Abbas AS, Ahmed LM, Mottaleb AS, et al. Study of Adsorption Characteristics of Co(II) on Eggshell Residue. Methods and Objects of Chemical Analysis. 2025;20(2):109-116.
45. Hateef, M.F., Alesary, H.F., Ahmed, L.M. and Barton, S., (2025). Synthesis of Spinal $CoFe_2O_4$ Nanoparticles Assitael with Cetramide and Applied in Removal of Direct Orange 39 Dye. Journal of Nanostructures, 15(2), pp.639-651.
46. De Castro MLFA, Abad MLB, Sumalinog DAG, Abarca RRM, Paoprasert P, de Luna MDG. Adsorption of Methylene Blue dye and Cu(II) ions on EDTA-modified bentonite: Isotherm, kinetic and thermodynamic studies. Sustainable Environment Research. 2018;28(5):197-205.
47. Theivarasu C, Mylsamy S. Removal of Malachite Green from Aqueous Solution by Activated Carbon Developed from Cocoa (Theobroma Cacao) Shell - A Kinetic and Equilibrium Studies. Journal of Chemistry. 2011;8(S1).
48. Al-Ahmed ZA. Surface methodology for optimized adsorption of hazardous organic pollutant from aqueous solutions via novel magnetic metal organic framework: Kinetics, isotherm study, and DFT calculations. J Mol Liq. 2024;409:125507.
49. Yatimzade, M. H., Ahmadpour, A., Ghahramaninezhad, M., & Sabzevar, A. M. (2024). Optimizing the efficient removal of ibuprofen from water environment by magnetic carbon aerogel: Kinetics, isotherms, and thermodynamic studies. Journal of Molecular Liquids, 408, 125337.
50. Saeed, S. I., Taresh, B. H., Ahmed, L. M., Haboob, Z. F., Hassan, S. A., & Jassim, A. A. A. (2021). Insight into the Oxidant Agents Effect of Removal and Photodecolorization of Vitamin B 12 Solution in Drug Tablets using ZrO_2. Journal of Chemical Health Risks, 11(4).
51. Mokhbi Y, Ghiaba Z, Akchiche Z, Ghedamsi R, Recioui B. Study of the adsorption mechanism of certain dyes from wastewater on commercial activated carbon using the Langmuir and Freundlich methods. Studies in Engineering and Exact Sciences. 2024;5(2):e5789.
52. Jaafar MT, Ahmed LM. Reduced the toxicity of acid black (nigrosine) dye by removal and photocatalytic activity of Tio2 and studying the effect of pH, temperatue, and the oxidant agents. AIP Conference Proceedings: AIP Publishing; 2020. p. 030034.
53. Nandiyanto, A. B. D., Putri, M. E., Fiandini, M., Ragadhita, R., Kurniawan, T., Farobie, O., & Bilad, M. R. (2024). Characteristics of Ammonia Adsorption on Various Sizes of Calcium Carbonate Microparticles from Chicken Eggshell Waste, Mor. J. Chem, 12(3), 1073-1095.
54. Al-Fiydh MN, Najm HF, Karam FF, Baqir SJ. Thermodynamics, kinetic study and equilibrium isotherm analysis of cationic dye adsorption by ternary composite. Results in Chemistry. 2024;10:101680.
55. Langmuir I. The Adsorption of Gases on Plane Surfaces of Glass, Mica and Platinum. Journal of the American Chemical Society. 1918;40(9):1361-1403.
56. Pourhakkak, P., Taghizadeh, A., Taghizadeh, M., Ghaedi, M. and Haghdoust, S., (2021). Fundamentals of adsorption technology. In Interface science and technology (Vol. 33, pp. 1-70). Elsevier.
57. Santos R, Silva ÉFM, Dantas EJM, Oliveira EDC, Simões TB, Araújo ÍRS, et al. Potential Reuse of PET Waste Bottles as a Green Substrate/Adsorbent for Reactive Black 5 Dye Removal. Water, Air, and Soil Pollution. 2020;231(11).
58. Temkin, M. J., & Pyzhev, V. (1940). Recent modifications to Langmuir isotherms. 217-222.
59. Khan TA, Khan EA, Shahjahan. Removal of basic dyes from aqueous solution by adsorption onto binary iron-manganese oxide coated kaolinite: Non-linear isotherm and kinetics modeling. Applied Clay Science. 2015;107:70-77.
60. Salih SJ, Abdul Kareem AS, Anwer SS. Adsorption of anionic dyes from textile wastewater utilizing raw corncob. Heliyon. 2022;8(8):e10092.
61. Kadhem, F.H., Ahmed, L.M., Abed, S.A., Tami, A.N. and Salleh, W.M.N.H.W., (2025). Green synthesis of CeO2 nanoparticle like-rose berry using ethanol Extract of Citrus aurantium peel and its potential in removal of organic waste, Al-Zahraa Journal for Health and Medical Sciences , 3(1), 50-76.
62. Georgi A, Kopinke F-D. Interaction of adsorption and catalytic reactions in water decontamination processes. Applied Catalysis B: Environmental. 2005;58(1-2):9-18.
63. Santos VP, Pereira MFR, Faria PCC, Órfão JJM. Decolourisation of dye solutions by oxidation with H2O2 in the presence of modified activated carbons. J Hazard Mater. 2009;162(2-3):736-742.
64. Fartode, A. P., & Parwate, D. V. (2014). Effect of H_2O_2 on UV Photolytic Remediation of Aqueous solutions of Methylene Blue. In IOsR Journal of Applied Chemistry, International Conference on Advances in Engineering & Technology , 69-72.
65. Alattar R, Saleh H, Al-Hilifi J, Ahmed L. Influence the addition of Fe^{2+} and H_2O_2 on removal and decolorization of textile dye (dispersive yellow 42 dye). Egyptian Journal of Chemistry. 2020;0(0):0-0.
66. Bello MM, Abdul Raman AA, Asghar A. A review on approaches for addressing the limitations of Fenton oxidation for recalcitrant wastewater treatment. Process Saf Environ Prot. 2019;126:119-140.
67. Borgohain X, Das E, Rashid MH. Facile synthesis of CeO_2 nanoparticles for enhanced removal of malachite green dye from an aqueous environment. Materials Advances. 2023;4(2):683-693.
68. Dadashi R, Bahram M, Farhadi K, Asadzadeh Z, Hafezirad J. Photodecoration of tungsten oxide nanoparticles onto eggshell as an ultra-fast adsorbent for removal of MB dye pollutant. Sci Rep. 2024;14(1).